THE JOURNAL OF PHYSICAL CHEMISTRY C

Article

pubs.acs.org/JPCC

Coverage-Dependent Structural Evolution in the Interaction of NO_2 with Au{111}

Tianfu Zhang,[†] Marco Sacchi, David A. King,[‡] and Stephen M. Driver*

Department of Chemistry, University of Cambridge, Lensfield Road, Cambridge, CB2 1EW, United Kingdom

Supporting Information

ABSTRACT: We have used low-temperature STM, together with DFT calculations incorporating the effects of dispersion forces, to study from a structural point of view the interaction of NO_2 with Au{111} surfaces. NO_2 adsorbs molecularly on Au{111} at 80 K, initially as small, disordered clusters at the elbows of the type-x reconstruction lines of the clean-surface herringbone reconstruction, and then as larger, ordered islands on the fcc regions. Within the islands, the NO_2 molecules define a $(\sqrt{3} \times 2)$rect. superlattice, for which we evaluate structural models. By around 0.25 ML coverage, the herringbone reconstruction has been lifted, accompanied by the formation of Au nanoclusters, and the islands have coalesced. At this stage, essentially the whole surface is covered with an overlayer consisting predominantly of domains of the $(\sqrt{3} \times 2)$rect. structure, but also containing less well-ordered regions. With further exposure, the degree of disorder in the overlayer increases; saturation occurs close to 0.43 ML.

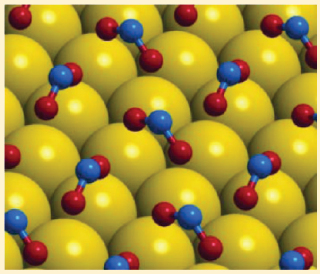

INTRODUCTION

In previous publications, we discussed aspects of the behavior of NO_2 and its interaction with CO on a single-crystal Au{111} surface in ultrahigh vacuum (UHV) conditions at temperatures in the range 78−160 K.[1,2] Key findings of those studies include: (1) mesoscopic self-organization of NO_2 islands within the herringbone reconstruction pattern at relatively low subsaturation coverages; (2) the emergence of strings of Au nanoclusters (the strings are typically of the order of 200 Å in length, containing around 20 clusters of 4−5 Au atoms), which form via a massively cooperative restructuring process as adjacent islands coalesce and locally lift the reconstruction; and (3) stabilization of CO on the surface at temperatures up to 145−160 K in the presence of NO_2.

Our interest in these phenomena is stimulated by the possibility, suggested by our previous work, that Au may be useful in low-temperature catalytic reactions involving NO_x. This idea couples the well-established catalytic activity of Au nanoparticles[3−5] with the fact that NO_2 is one of only very few species that readily adsorb on Au{111}. A strong motivation for studying the behavior of nitrogen oxides on metal surfaces is the importance of de-NO_x catalysis in controlling environmentally damaging vehicle exhaust and flue gas emissions.

In this work, we follow up our initial reports by examining in more depth the behavior of NO_2 on Au{111} as a function of coverage. Using a UHV low-temperature scanning tunnelling microscope (LT-STM), we have monitored structural changes of the substrate occurring at around 80 K, from initial adsorption through to saturation of the adsorbate. We have used first-principles modeling within the framework of density functional theory (DFT), incorporating van der Waals (vdW) interactions, to investigate the nature of the ordered NO_2 overlayers that form. We focus particularly on how the initial adsorption is influenced by the herringbone pattern, and also on the nature of the saturated overlayer just prior to its interaction with CO in our previously reported coadsorption experiments.

EXPERIMENTAL SECTION

The Au{111} surface was cleaned in UHV by repeated cycles of Ar^+ ion sputtering and annealing, until an Auger electron spectrum free of contaminant peaks and a sharp low-energy electron diffraction (LEED) pattern exhibiting satellite spots characteristic of the clean-surface herringbone reconstruction were obtained.

Reflection−absorption infrared spectroscopy (RAIRS) measurements were performed using a Mattson Galaxy 6021 FTIR spectrometer and MCT detector, coupled via KBr windows to a UHV system equipped with standard preparation and characterization facilities. In the RAIRS experiments, NO_2 was adsorbed by background exposure to NO_2 gas with the surface at 120 K.

STM measurements were performed using an Omicron LT-STM installed in a separate UHV system. In the STM experiments, NO_2 was adsorbed by backfilling the STM chamber with NO_2 gas, with the sample in the STM sample stage at around 80−85 K (the temperature increased slowly while the cryoshield doors were open). Because of the cryopumping effect of the STM cryostat, which fully encloses the STM, nominal exposures in Langmuir (1 L = 10^{-6} Torr s) cannot be directly compared between experiments in the two UHV systems. All images were obtained in constant-current (topographic) mode using an electrochemically etched W tip, once the sample had stabilized at 78 K. The images shown were

Received: October 11, 2011
Revised: February 2, 2012
Published: February 5, 2012

recorded at −1.0 V sample bias and 0.1 nA tunnelling current, conditions which were found to give stable, high-resolution imaging with minimal perturbation of the molecular overlayer.

Calculation Details. Our first-principles calculations are based on DFT as implemented in the CASTEP code, which employs plane waves and periodic boundary conditions.[6] We have discussed the details of this methodology in several recent studies.[7−10] In this section, we report only the most important features of the theoretical method applied, and highlight the differences between this work and the calculations reported in our previous study on CO/NO_2 coadsorption on Au{111}.[1]

We simulate the unreconstructed Au{111} surface as a periodically repeated $(\sqrt{3} \times 2)$rect. slab (except where otherwise stated), constituted of four atomic layers. We fix the position of the bottom two layers as in the ideal Au bulk crystal, and allow the top two layers to relax during structural optimization of the surface and adsorbate. To avoid spurious interactions between the periodically repeated slabs, a vacuum layer of thickness equivalent to seven atomic layers is added above the Au{111} slab. Total energy calculations are performed using the generalized gradient approximation with the PW91 exchange-correlation functional[11] and Vanderbilt ultrasoft pseudopotentials.[12] Integration of the wave function is over a $(6 \times 6 \times 1)$ Monkhorst-Pack[13] grid of k-points in reciprocal space, and we use a cutoff energy of 340 eV. In the following sections, we will discuss the effect of incorporating spin polarization and van der Waals (vdW) corrections on the binding energy and relative stability of adsorbed NO_2 phases.

The well-known inability of DFT to account for long-range dispersion force interactions has encouraged the development of several alternative methods to correct—completely or at least in part—for this fundamental weakness of the DFT methodology. In this study, we employed the semiempirical correction method (DFT+D) implemented by Ortmann, Bechstedt, and Schmidt.[14] This methodology is based on the computationally efficient semiempirical pair-potential method, and allows us to estimate the relative importance of dispersion interactions between NO_2 molecules for the 0.25−0.5 ML coverage range. For all self-consistent energy calculations, we use an electronic energy tolerance of 10^{-6} eV, while the force tolerance during geometry optimization was 5×10^{-5} eV $Å^{-1}$. In some cases, the energy difference between alternative structures that we discuss are rather small (of the order of 10 meV). DFT errors are hard to estimate; we discuss the level of agreement between our calculated stabilities and experimental observations in detail below. Nevertheless, we note that, at least in some well-behaved systems, the relative adsorption energies of different sites can be calculated with great accuracy (see, e.g., ref 7).

RESULTS AND DISCUSSION

RAIRS Measurements of NO_2 Adsorption. Figure 1 shows a RAIR spectrum obtained after exposing the clean Au{111} surface at 120 K to 0.15 L of NO_2. The spectrum is dominated by a single peak at 1180 cm^{-1}: the symmetric stretch, $\nu_s(NO_2)$, of NO_2 bonded to the surface through the two O atoms in a chelated configuration. The peak at 1900 cm^{-1}, arises from the symmetric stretch $\nu(NO)$ of N_2O_3, but its intensity is very low, and other peaks associated with N_2O_3 and N_2O_4 are absent, indicating that the NO_2 adlayer is essentially pure. In ref 15, pure NO_2 RAIR spectra are shown only for surfaces heated to 172 K or more to desorb NO from N_2O_3; all spectra obtained directly after dosing at 85 K in that work

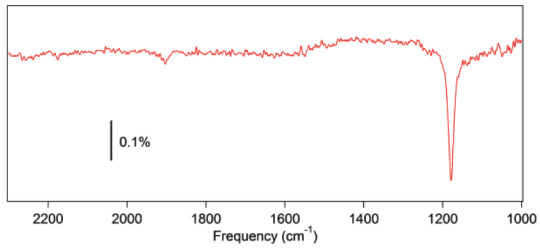

Figure 1. RAIR spectrum obtained after exposing Au{111} at 120 K to 0.15 L of NO_2.

contain pronounced N_2O_3-related peaks, but the lowest coverage for which a spectrum is shown is 0.5 ML. Our pure NO_2 spectrum, obtained by exposure at 120 K, evidently corresponds to a coverage sufficiently low that N_2O_3 has not formed to any significant extent; this behavior is consistent with the TPD spectra of ref 16, and indeed with other previously published RAIRS data.[17] The coverage at this exposure cannot be higher than around 0.15 ML (using the rule of thumb that 1 L gives 1 ML if the sticking probability is 1); on the basis of ref 16, we estimate that the coverage may actually be as low as around 0.03 ML. This implies that STM images obtained at correspondingly low NO_2 coverages should represent pure NO_2, free of N_2O_3.

STM Observations of NO_2 Overlayer up to 0.25 ML. The STM image in Figure 2(a) shows Au{111} after the very lowest exposures to NO_2 at around 80 K. The herringbone reconstruction pattern is clearly visible.[18−22] Small clusters, each containing a few molecules, decorate the majority of the elbows of the type-x reconstruction lines.[23] The elbows correspond to the locations of threading dislocations, occurring where the Burger's vector of the reconstruction line changes direction, and associated with a local change in the top-layer packing density. These points commonly act as nucleation sites when depositing metals such as Ni, Co, and Fe.[24−27] The clusters at the "bulged" elbows are systematically larger (typically 7 molecules) than those at the "pinched" elbows (4 molecules), reflecting the different nature of the point defects at these two types of elbow.

At this initial stage, we find occasional larger clusters. An example, containing around 40 individually resolved NO_2 molecules, is shown at high resolution in Figure 2(b). These occur exclusively on the wider parts of the fcc regions adjacent to the "pinched" elbows. Within the clusters, the molecules are not well-ordered, although the beginnings of ordering, into both 1-D linear chains and a 2-D overlayer, are apparent. The molecules have some degree of mobility at 78 K, as seen from the slight streaking and from the fact that a few molecules have hopped in the interval between recording successive scan lines, appearing as semicircular "half-molecules". These clusters are the nuclei for subsequent growth, as we show below.

With continuing exposure to NO_2 at around 80 K, adsorbate islands appear, growing exclusively on fcc regions of the herringbone reconstruction pattern (Figure 3). Within the islands, the molecules define a rectangular superlattice of $(\sqrt{3} \times 2)$rect. periodicity, consistent with 0.25 ML local coverage. We discuss the detailed structure of this phase below. Each island typically contains multiple rotational and/or translational domains of the $(\sqrt{3} \times 2)$rect. structure. The example in Figure 3 contains all three rotational domains; translational domain boundaries can be seen in images discussed later (e.g., Figure 4(b)).

dx.doi.org/10.1021/jp2097586 | J. Phys. Chem. C 2012, 116, 5637−5645

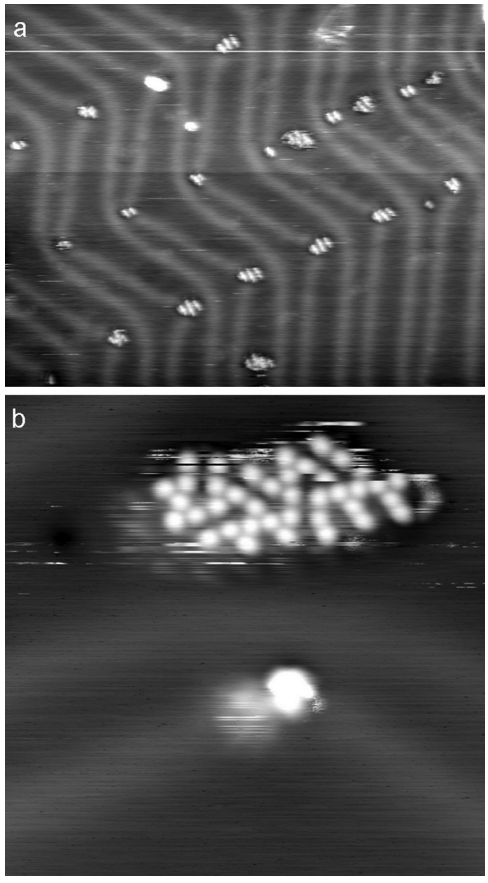

Figure 2. STM images of Au{111} after very low exposures at 80 K to NO_2. (a) NO_2 clusters at the elbows of the clean-surface herringbone reconstruction (500 × 400 Å^2, greyscale range 1 Å). (b) Larger cluster on fcc region, showing some 1-D and 2-D order; faint "ghost" images are attributed to a slight double tip (100 × 100 Å^2, 1.5 Å).

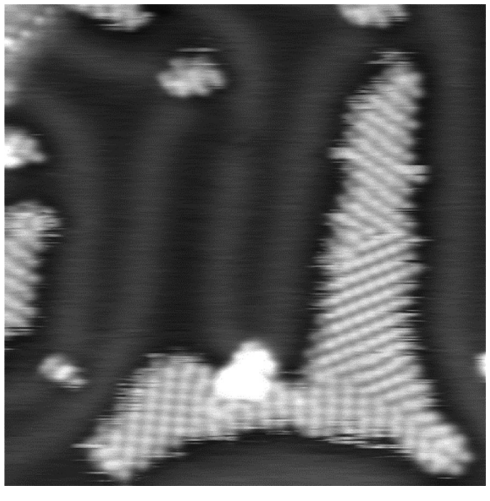

Figure 3. STM image showing NO_2 island that has grown along fcc regions of reconstructed Au{111}. The island contains all three rotational domains of the $(\sqrt{3} \times 2)$rect.-NO_2 structure (200 × 200 Å^2, 1.2 Å).

As the coverage increases, the islands grow and start to coalesce. We discussed this in detail in ref 2 and summarize the earlier findings here for completeness. A key point is that the islands are arranged in mesoscopically ordered patterns, driven by interactions between their local stress fields. Accordingly,

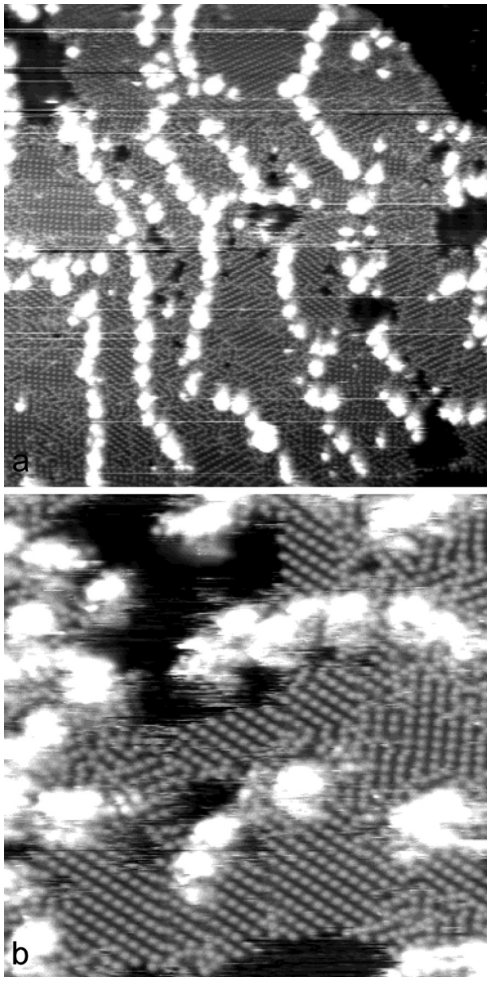

Figure 4. STM images of Au{111} showing NO_2 overlayer at around 0.25 ML overall coverage. (a) Large-area image showing almost complete coalescence of NO_2 islands, and strings of clusters (white) marking the initial positions of reconstruction lines (see text). There is a step edge at top right. (500 × 500 Å^2, 2.5 Å) (b) High resolution image showing arrangement of $(\sqrt{3} \times 2)$rect.-NO_2 domains and less well-ordered regions within the overlayer (200 × 200 Å^2, 1.5 Å).

neighboring islands, situated in successive fcc regions of the substrate herringbone pattern, extend along the fcc strips alternately to one side then the other of the domain boundary that is defined by the row of elbows in the reconstruction lines. When these islands coalesce across the intervening hcp region, the reconstruction is locally lifted through a massively cooperative restructuring process, the resulting larger island sitting on an extended fcc region. The excess Au atoms, ejected from the surface layer by this process, agglomerate into nanoclusters of 4−5 atoms, without significant diffusion away from the point at which they were ejected. The nanoclusters are therefore arranged in strings, typically some 200 Å long, marking the approximate positions of reconstruction lines just prior to the atoms' ejection.

STM Observations of NO_2 Overlayer: 0.25 ML and Beyond. Figure 4 shows STM images of the surface when the overall coverage is close to 0.25 ML, at which point the NO_2 islands have mostly coalesced to form a near-continuous overlayer, and very little bare Au substrate is left exposed. By this stage, the lifting of the reconstruction is essentially complete. The overlayer comprises many small domains of

dx.doi.org/10.1021/jp2097586 | J. Phys. Chem. C 2012, 116, 5637−5645

the $(\sqrt{3} \times 2)$rect. structure, together with various point and line defects and small, less well-ordered regions. As seen at lower coverages in our previous work,[2] strings of Au nanoclusters decorate the overlayer, marking out the approximate final positions of reconstruction lines in the herringbone structure prior to the reconstruction being lifted.

We note that in previous studies, no LEED pattern corresponding to the $(\sqrt{3} \times 2)$rect. phase has been reported. In our STM investigation, we were unable to check the LEED pattern without the sample warming above the desorption temperature for NO_2; in LEED measurements made at low temperature during our RAIRS investigation, we did not observe any superstructure spots appearing as the herringbone reconstruction was lifted. The size of individual $(\sqrt{3} \times 2)$rect. domains in the STM images is typically rather smaller than the LEED transfer width (which is of the order of 100 Å),[28] but one might nevertheless expect to see a LEED pattern consistent with superposition of the individual patterns of the three rotational domains. The most likely explanation for the failure to observe a $(\sqrt{3} \times 2)$rect. LEED pattern is that the NO_2 overlayer is highly susceptible to electron-beam damage under typical LEED operating conditions.

In general, the tunnelling signal became noisy and unstable when trying to image the surface after very high exposures to NO_2, and we were unable to record high-resolution images. We attribute this to the onset of multilayer formation, leading to a surface too unstable at 78 K to be imaged by STM. Figure 5

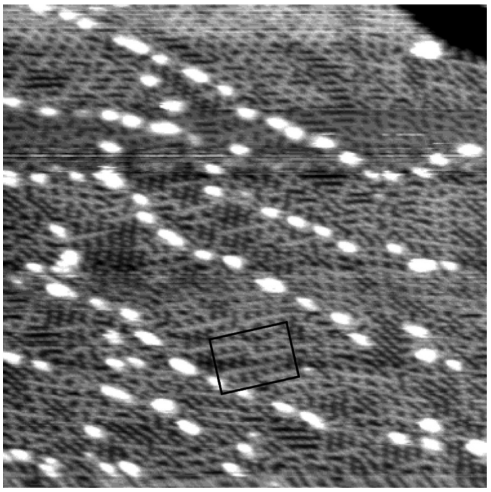

Figure 5. STM image showing partially ordered NO_2 overlayer and strings of Au nanoclusters (white) on Au{111} after exposure at 80 K to NO_2 beyond the 0.25 ML point (300 × 300 Å^2, 3 Å). A possible structural model for the boxed area is discussed in the text.

shows one of the very few images in which acceptable resolution was obtained after significant NO_2 exposure beyond the 0.25 ML point. Inspection of the image indicates that the coverage is >0.25 ML and <0.5 ML, while the marginal resolution suggests that we are close to the onset of multilayer formation, which is known to be at around 0.4 ML.[15,16] The detailed structure is relatively difficult to discern, but its appearance is qualitatively similar to the less well-ordered regions seen at 0.25 ML. We suggest that this overlayer is based on the $(\sqrt{3} \times 2)$rect. phase, but with a significant fraction of $(\sqrt{3} \times 2)$rect. meshes containing a second NO_2 molecule, and with a significant degree of disorder. We discuss a possible structure of this phase below.

Structure of the $(\sqrt{3} \times 2)$rect. Phase: Experimental Clues. The chelated bonding configuration is well-established from HREELS and RAIRS studies,[15−17] and the bridge-bonding site from previous theoretical calculations.[29] On the basis of this information and the $(\sqrt{3} \times 2)$rect. periodicity, two possible models emerge for this phase at 0.25 ML coverage. In the "inline-molecule" model, Figure 6(a), all molecules are aligned

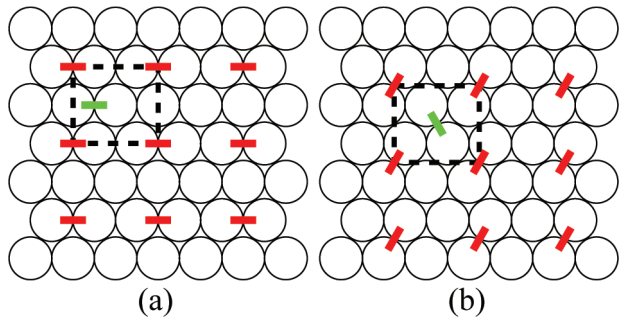

Figure 6. Schematic structural models for the $(\sqrt{3} \times 2)$rect.-NO_2 phase on Au{111} at 0.25 ML coverage. (a) The inline-molecule model. (b) The rotated-molecule model (see text). The $(\sqrt{3} \times 2)$rect. unit mesh is marked (dotted black rectangle). Orange bars represent the O−N−O molecular plane, with NO_2 occupying bridge sites bonding to Au atoms in a chelated configuration through the O atoms. The green bars represent a second NO_2 molecule in the same bonding configuration, corresponding to an 0.5 ML phase. In the rotated-molecule structure, the second NO_2 molecule must be in the center of the mesh, whereas in the inline-molecule structure, it must be off-center.

with the O−N−O plane parallel to the long side of the unit mesh, whereas in the "rotated-molecule" model, the alignment is staggered as shown in Figure 6(b).

The NO_2 bonding site and configuration cannot, of course, be measured directly from the STM data. In common with most such experiments, tunnelling conditions suitable for obtaining atomic resolution of the substrate perturb the molecular overlayer; the method of switching tunnelling conditions and extrapolating a lattice, used by Bradshaw and co-workers for isolated molecules,[30] is not feasible for a surface of this complexity. Nor is there any asymmetry in the imaging of individual NO_2 molecules that might indicate the orientation of the projected O−N−O plane.

Evidence to distinguish between these models can nevertheless be found in the STM data, by examining the point and line defects. Figure 7 shows a characteristic line defect: a translational domain boundary, running in a $\langle 2\ 1\ -3 \rangle$ direction defined by the diagonal of the $(\sqrt{3} \times 2)$rect. unit mesh. Models consistent with the relative alignment of the $(\sqrt{3} \times 2)$rect. lattices of the two domains are shown in Figure SI-1 of the Supporting Information, SI. It can be seen that both the inline-molecule and one of the rotated-molecule models are consistent with the experimental data. However, the mirror-equivalent rotated-molecule model is not compatible with this orientation of boundary, since in this case the closely positioned neighbors at the boundary would involve one O atom from each of two NO_2 molecules being bonded to the same Au atom.

A point defect occurs when a second NO_2 molecule is added to the $(\sqrt{3} \times 2)$rect. unit mesh, as shown schematically in Figure 6. If added to the rotated-molecule structure with the same bonding configuration, the second molecule lies in the

dx.doi.org/10.1021/jp2097586 | J. Phys. Chem. C 2012, 116, 5637−5645

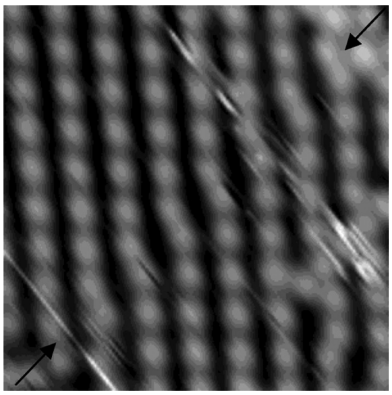

Figure 7. STM image of translational domain boundary, running in ⟨2 −1 3⟩ direction (marked by arrows), within ($\sqrt{3} \times 2$)rect.-NO_2 phase on Au{111} at 0.25 ML. The STM image has been rotated to make the orientation consistent with the schematics in Figure SI-1. (50 × 50 Å^2, 1.5 Å).

center of the mesh, whereas it lies off-center if added to the inline-molecule structure. The STM images in Figure 8 show

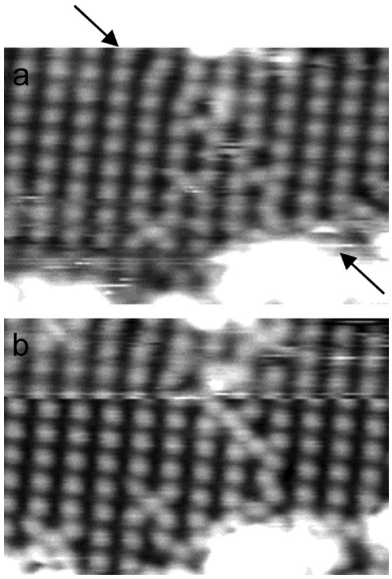

Figure 8. STM images of ($\sqrt{3} \times 2$)rect.-NO_2 phase on Au{111} showing decorated ($\sqrt{3} \times 2$)rect. unit meshes and decorated ⟨2 1 −3⟩ translational domain boundary (position indicated by arrows in (a). The two images of the same region were recorded consecutively, (b) following (a), and show subtle changes associated with NO_2 mobility. A spontaneous tip change occurred near the top of the latter image. (75 × 50 Å^2, 1.5 Å).

examples of a ($\sqrt{3} \times 2$)rect. unit mesh decorated with an additional NO_2 molecule. These features occur infrequently, but in each case the additional molecule lies in the center of the mesh, consistent with the rotated-molecule structure but not the inline-molecule structure. The alternative possibility is that the additional molecule is not bonded in the same configuration: for the inline-molecule structure, this would imply atop site occupation. This seems intuitively unlikely, and one would expect inequivalent species to image differently, an effect not supported by the data. DFT calculations, described below, also disfavor mixed site occupation in the ($\sqrt{3} \times 2$)rect. phase. In summary, these point defects are best explained in terms of the rotated-molecule structure of Figure 6(b).

Figure 8 also shows a translational domain boundary, similar to that in Figure 7 but decorated with additional NO_2 molecules. Models for these decorated boundaries, based on the inline-molecule and rotated-molecule meshes, and assuming that all molecules adopt the same bonding configuration, are shown in Figure SI-2 of the SI. In the STM images, the additional molecules appear to be aligned with the terminal NO_2 molecules in the lower domain, favoring the decorated rotated-molecule boundary model in Figure SI-2(a) of the SI. This model places NO_2 molecules with a sawtooth arrangement in a ⟨2 1 −3⟩ direction, a motif that we will see again later. The similarity between this decorated boundary and an 0.5 ML rotated-molecule ($\sqrt{3} \times 2$)rect. mesh is apparent.

Figure 9 shows examples of another kind of line defect, also having a ⟨2 1 −3⟩ orientation, seen frequently in the images.

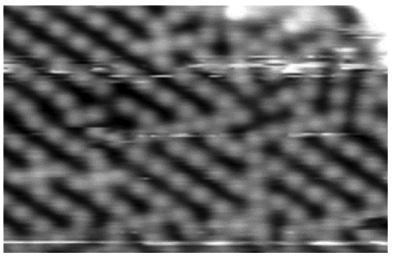

Figure 9. STM image of a typical region of the NO_2 overlayer on Au{111} at 0.25 ML, in which there is significant disruption to the ($\sqrt{3} \times 2$)rect. structure, including ⟨2 1 −3⟩ line defects whose structure is discussed in the text. (78 × 50 Å^2, 1.5 Å).

These again separate two translational domains, as seen from the displacements between the ($\sqrt{3} \times 2$)rect. lattices to either side of the boundaries. The two point defects (Figure 9, lower left) indicate that the structure is based on the rotated-molecule model, as before. Figure SI-3 of the SI shows alternative models for this region of the surface, in which the relative positions of the molecules are derived directly from the STM data, and this overlayer configuration is placed on the substrate lattice with different registries.

In the model in Figure SI-3(a) of the SI, all ($\sqrt{3} \times 2$)rect. regions adopt the preferred rotated-molecule model, and the two point defects at lower left are consistent with this. However, when we examine the line defects, which are oriented in ⟨2 1 −3⟩ directions, it is clear that the NO_2 molecules alternate between bridge and atop sites. Occupation of atop sites is surprising for NO_2, and inconsistent with all other evidence. Additionally, one would expect the very different bonding to cause dissimilar heights in the STM images. Such contrast changes are not, however, apparent.

The same inconsistency arises in the model in Figure SI-3(b) of the SI. This is again based on the rotated-molecule model, but the mirror-equivalent domain of that in Figure SI-3(a) of the SI. Moreover, this registry leads to the domain in the upper right-hand corner corresponding to the inline-molecule model, instead of the rotated-molecule model, and to at least one point defect involving two NO_2 molecules bonding to the same Au atom (center left).

The only way to bring all molecules in the ⟨2 1 −3⟩ line defects into bridge positions, consistent with the previous model for ⟨2 1 −3⟩ boundaries, is to base the overall structure on the inline-molecule model, as shown in Figure SI-3(c) of the

dx.doi.org/10.1021/jp2097586 | J. Phys. Chem. C 2012, 116, 5637−5645

SI. However, this is inconsistent with the two point defects (lower left). Overall, we conclude that the balance of probability is that the model in Figure SI-3(a) of the SI is the correct one, and that these ⟨2 1 −3⟩ boundaries do indeed contain NO_2 molecules in atop positions. This is puzzling, as it seems to be inconsistent with the balance of evidence for the point defects; we address this further using DFT below.

Structure of the ($\sqrt{3} \times 2$)rect. Phase: DFT Modeling. To put the structural interpretation on a firmer footing, we performed first-principles calculations for the ($\sqrt{3} \times 2$)rect. phase of NO_2 on Au{111} at coverages between 0.25 and 0.5 ML, as well as NO_2 in a (3,1;1,3) cell at 0.125 ML. Previous theoretical and experimental studies[15,16,29] concluded that the most favorable adsorption site for NO_2 on Au{111} is the bridge site between two nearest-neighbor Au atoms, with the NO_2 in the so-called chelated configuration, bonding to the surface through the O atoms. Although we mainly focus our DFT study on this chelated bridge configuration, we have also investigated the relative stability of domains containing NO_2 molecules in alternate bridge and atop sites, in light of the STM observations described above.

Table 1 reports the calculated binding energy (E_a) for a single NO_2 molecule adsorbed within a Au{111}-($\sqrt{3} \times 2$)rect.

Table 1. Results of DFT Calculations for Au{111}-($\sqrt{3} \times 2$)rect.-NO_2 Structure at 0.25 ML Coverage (i.e., One Molecule Per Unit Mesh; Models Shown in Figure 10)[a]

Au{111}-($\sqrt{3} \times 2$) rect.	E_a (eV)	ΔE_a (eV)	
NO_2 *rotated*	0.699	0.000	DFT (GGA)
NO_2 *inline*	0.677	0.021	
NO_2 *rotated*	0.706	0.000	DFT (GGA) + spin-polarization
NO_2 *inline*	0.678	0.029	
NO_2 *rotated*	0.821	0.000	DFT+D (GGA) + spin-polarization
NO_2 *inline*	0.793	0.028	

[a]Calculated adsorption energy (E_a); adsorption energy relative to the most stable configuration (ΔE_a); and level of theory utilized. We use PW91 for the GGA xc-functional.[11] DFT+D means DFT with PW91 xc-functional and the semi-empirical correction for long-range dispersion forces obtained with the method of Ortmann et al.[14].

unit cell (i.e., 0.25 ML coverage), with the difference in binding energy between the two most stable configurations (identified as *rotated* and *inline*, Figure 10) indicated as ΔE_a. The basic

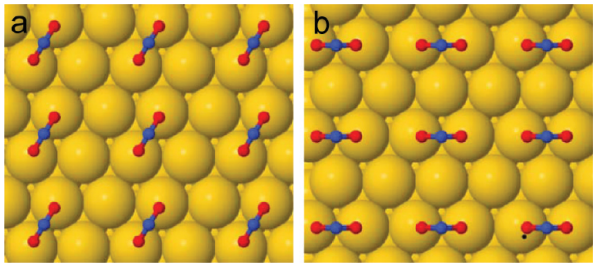

Figure 10. Models for ($\sqrt{3} \times 2$)rect.-NO_2 phase on Au{111} at 0.25 ML used in the DFT calculations. These models are equivalent to those shown schematically in Figure 6. (a) The rotated-molecule phase; (b) the inline-molecule phase.

DFT calculation indicates that the absolute binding energy is around 0.7 eV, which is quite consistent with estimates based on TPD experiments (0.61 eV).[16,17] The binding energies are essentially unaffected by accounting for spin-polarization. The rotated-molecule model is marginally the more stable of the two, in agreement with the STM indications; the energy difference is about 20−30 meV. It is clear that when the molecules can choose between very similar surface orientations in their self-assembly, even a relatively small contribution from long-range electrostatic effects can favor one phase over another.

Accounting for vdW corrections (DFT+D in Table 1) increases the absolute binding energy of NO_2 by 0.12 eV for both models. Covalent bonding between metal and molecule is therefore the dominant interaction, as one would expect. Nevertheless, it is striking that, even for a small molecule like NO_2, vdW interactions can account for as much as 15% of the total binding energy. In this particular case, however, vdW interactions do not influence the *relative* stability of the two configurations.

The STM data reveal islanding behavior at low coverages, implying attractive lateral interactions between NO_2 molecules. In order to estimate the existence of a driving force that favors island formation over a dilute phase, we have calculated the binding energy for a single NO_2 molecule in a (3,1;1,3) supercell, corresponding to a coverage of 0.125 ML (Table 2),

Table 2. Results of DFT Calculations for 0.125 ML NO_2 on Au{111}, with a Single Molecule in a (3,1;1,3) Unit Mesh on Au{111}[a]

structure	E_a (eV)	θ (ML)	
NO_2 *rotated-* (3113).	0.688	0.125	DFT (GGA) + spin-polarization
NO_2 *rotated-* (3113).	0.797	0.125	DFT+D (GGA) + spin-polarization

[a]Calculated adsorption energy (E_a), coverage (θ) and level of theory utilized.

as a model for isolated molecules. The 0.125 ML structure is less stable than the 0.25 ML ($\sqrt{3} \times 2$)rect. rotated-molecule phase, by 18 meV in the GGA calculations and by 24 meV when accounting for long-range dispersion forces. There is thus weak lateral attraction even in the absence of dispersion forces, and this is strengthened by vdW attractions.

We have also performed calculations with a second NO_2 molecule added to the Au{111}-($\sqrt{3} \times 2$)rect. unit mesh, giving 0.5 ML coverage, in order to investigate how the degree of interaction between adjacent molecules is affected by doubling the adsorbate concentration. This is relevant in the context of the occasional unit meshes that contain two NO_2 molecules seen in the STM data, and also the observation in previous studies that the pure NO_2 layer appears to saturate at around 0.4 ML, further exposure leading to N_2O_3 and N_2O_4 formation.[15,16]

0.5 ML models based on the "rotated-molecule" and "inline-molecule" structures discussed above are shown in Figure 11. When we compare the relative binding energies per molecule for these two structures, we find that the rotated-molecule phase is more stable by 0.167 eV than the inline-molecule phase at 0.5 ML (Table 3). We attribute this to the greater nearest-neighbor intermolecular spacing in the former. This supports the preference for this model reached from the characteristics of the isolated 0.5 ML unit meshes in the STM data. Adding vdW corrections does not significantly modify the relative stability of these two structures.

dx.doi.org/10.1021/jp2097586 | J. Phys. Chem. C 2012, 116, 5637−5645

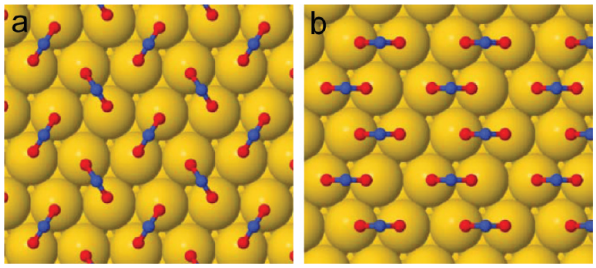

Figure 11. Models for $(\sqrt{3} \times 2)$rect.-NO_2 phase on Au{111} at 0.5 ML used in the DFT calculations, with all molecules in chelated bonding configuration in bridge sites (compare Figure 6). (a) The rotated-molecule phase; (b) the inline-molecule phase.

Table 3. Results of DFT Calculations for Au{111}-$(\sqrt{3} \times 2)$rect.-NO_2 Structure at 0.5 ML Coverage (i.e., Two Molecules Per Unit Mesh; Models Shown in Figure 11)[a]

structure	E_a (eV)	ΔE_a (eV)	
$2NO_2$ *rotated* - $(\sqrt{3} \times 2)$ rect.	0.661	0.000	DFT (GGA) + spin-polarization
$2NO_2$ *inline* - $(\sqrt{3} \times 2)$ rect.	0.494	0.167	
$2NO_2$ *rotated* - $(\sqrt{3} \times 2)$ rect.	0.812	0.000	DFT+D (GGA) + spin-polarization
$2NO_2$ *inline* - $(\sqrt{3} \times 2)$ rect.	0.640	0.172	

[a]Calculated adsorption energy (E_a); adsorption energy relative to the most stable configuration (ΔE_a) for the same unit mesh; and level of theory utilized.

The absolute binding energy per molecule for the rotated-molecule phase at 0.5 ML is only 45 meV lower than at 0.25 ML in the basic spin-polarized calculation, and this energy difference becomes essentially negligible if we include dispersion interactions (Table 3). The calculations thus indicate that there is no strong lateral repulsion between adjacent NO_2 molecules at this coverage: the presence of the significant long-range attraction between isolated molecules that leads to islanding, coupled with vdW attractions between adjacent molecules, evidently overcome the weak dipole−dipole repulsion in this high-coverage phase.

For completeness, we have also tested 0.5 ML structures based on the "inline-molecule" phase, in which one NO_2 molecule is in the bridge chelated position considered so far, while the second NO_2 molecule is in an atop site, either bonded to the surface through the O atoms as before, or in an inverted configuration bonded through the N atom (Figure 12). This would, in principle, allow a second molecule to be in a central position within the inline-molecule structure, suggesting an alternative interpretation of the STM data. Compared to the preferred, rotated-molecule configuration discussed above, however, both of these structures are much less stable, the inverted atop model by 0.219 eV, the noninverted atop model by 0.29 eV. Indeed, when the atop NO_2 is inverted, all molecules become azimuthally twisted away from their starting positions when the calculation converges (Figure 12). Moreover, one might expect the inequivalent species to image at different apparent heights in the STM, and the molecule in the inverted configuration to image with a different shape. Neither of these expectations is supported by the data.

Structure of the High-Coverage Phase and Boundaries. The reduced order seen in our STM images of the surface

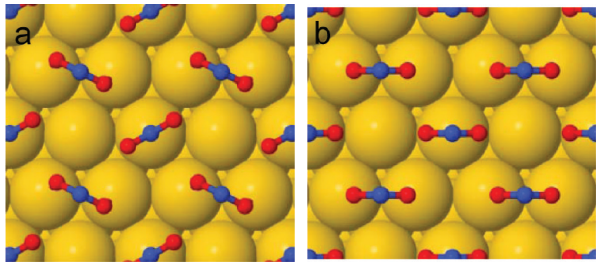

Figure 12. Models for $(\sqrt{3} \times 2)$rect.-NO_2 phase on Au{111} at 0.5 ML, with molecules occupying mixed bridge and atop sites. The molecule in the atop site may be bonded (a) through the N atom, or (b) through the two O atoms. The structures are shown after convergence of the DFT calculation: the azimuthal twist in the molecules seen in (a) is a result of energy minimization.

above 0.25 ML NO_2 coverage (Figure 5) is consistent with the findings of earlier studies, in which the saturation coverage of a pure NO_2 chemisorbed overlayer was measured to be around 0.4 ML: a multilayer, in the form of N_2O_3 or N_2O_4, forms beyond that coverage.[16] The experimental evidence—from the earlier studies and from our STM investigation—is that a pure NO_2 overlayer with the full 0.5 ML coverage is not reached.

The surface in Figure 5 is quite heterogeneous, and the images only marginally resolved, so it is difficult to be definitive about structural details. However, Figure SI-4 of the SI shows a plausible structure for a selected area of the image in Figure 5. The bright, unresolved lines in the image are interpreted as the ⟨2 1 −3⟩ sawtooth rows of NO_2 molecules discussed above. Within this model can be found $(\sqrt{3} \times 2)$rect. unit meshes containing both one and two NO_2 molecules, both of rotated-molecule type. The overall coverage must therefore be intermediate between 0.25 and 0.5 ML, as expected.

As an idealized model of the surface at this stage, we have calculated the binding energy of NO_2 at intermediate coverage (0.375 ML) using a (3,1;1,3) supercell with 3 molecules per cell (Figure 13), giving a periodic phase based on the proposed

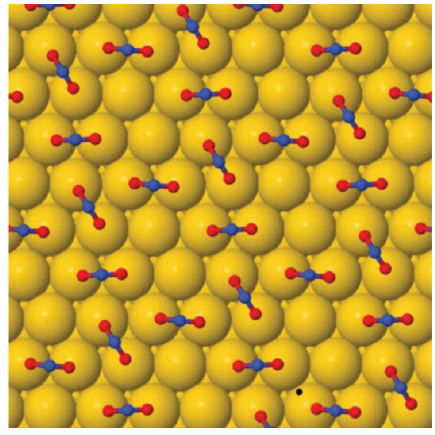

Figure 13. Idealized, periodically ordered model used for DFT calculations of high-coverage NO_2 phase on Au{111} based on 0.375 ML coverage in a (3,1;1,3) unit mesh.

structure in Figure SI-4 of the SI. Neglecting dispersion forces, the binding energy is close to that of the 0.5 ML rotated-molecule phase (5% lower), whereas when we include vdW attractions, the binding energy is practically indistinguishable (within 2%) from those of the 0.25 and 0.5 ML coverage phases (Table 4). The almost identical binding energies per molecule

dx.doi.org/10.1021/jp2097586 | J. Phys. Chem. C 2012, 116, 5637−5645

Table 4. Results of DFT Calculations for 0.375 ML NO_2 on Au{111}, with Three Molecules in a (3,1;1,3) Unit Mesh[a]

structure	E_a (eV)	θ (ML)	
$3NO_2$ *rotated*-(3113).	0.669	0.375	DFT (GGA) + spin-polarization
$3NO_2$ *rotated*-(3113).	0.806	0.375	DFT+D (GGA) + spin-polarization

[a]Calculated adsorption energy (E_a), coverage (θ) and level of theory utilized.

at different coverages are consistent with the observation of coexistent NO_2/Au{111}-($\sqrt{3} \times 2$)rect. unit meshes having either one or two molecules per mesh, and with some limited regions in which the overlayer resembles the 0.375 ML (3,1;1,3) structure.

On the basis of the foregoing discussion, we see that first-principles modeling at the highest currently available level of DFT successfully accounts for much of the experimentally observed behavior, but is unable to account fully for all features seen in the STM data. DFT shows very little destabilization between 0.25 and 0.5 ML, even when dispersion forces are taken into account, if all molecules adopt the chelated bridge-bonded configuration based on the preferred rotated-molecule structure. It is possible that calculations for the multilayer phase would reveal it to be more stable than the single-layer phase at coverages above 0.4 ML. However, such calculations would be prohibitively expensive at the present time, especially in the absence of experimental characterization of the multilayer structure.

In this context, we also mention a key finding of our experiments and DFT calculations involving coadsorption of CO with NO_2 on Au{111}.[1,31] In those experiments, NO_2 overlayers similar to that shown in Figure 5 were exposed at 80 K to CO. Thereafter, the surface was found to be almost entirely covered by large domains of a CO/NO_2 coadsorbed overlayer with ($\sqrt{7} \times \sqrt{7}$)R19.1° periodicity and containing three NO_2 molecules per unit mesh, i.e., an NO_2 coverage of 3/7 or 0.43 ML. This demonstrates that the NO_2 precoverage prior to exposure to CO was essentially 0.43 ML, which is consistent with the previously reported saturation value of around 0.4 ML. Very small fractional areas at domain boundaries of this coadsorption phase were covered by a pure NO_2 phase. These regions were found to consist of the 0.5 ML ($\sqrt{3} \times 2$)rect.-$2NO_2$ structure discussed above: evidently this phase *does* form, but only in very small regions stabilized by the surrounding coadsorbed phase.

Finally, we address the STM evidence suggesting ⟨2 1 −3⟩ boundaries containing mixed bridge and atop sites for NO_2 (Figure 9). For this purpose, we calculate the binding energy per molecule in the structure shown in Figure 14. This is a ($\sqrt{7} \times \sqrt{7}$)R19.1° unit mesh containing three NO_2 molecules, corresponding to a coverage of 3/7 or 0.43 ML. The molecules alternate between atop and bridge occupation in one of the ⟨2 1 −3⟩ directions. The calculated binding energies per molecule are 0.511 eV without vdW forces, or 0.652 eV with vdW forces. This represents a significant destabilization relative to either the 0.375 ML (3,1;1,3) or the 0.5 ML ($\sqrt{3} \times 2$)rect. rotated-molecule phases with pure bridge-site occupation, which is presumably related to the relatively unfavorable atop site occupation of one of the NO_2 molecules. As such, DFT is unable to shed light on this aspect of the STM data. Further experiments would be necessary to confirm or disprove this site assignment based on STM image interpretation.

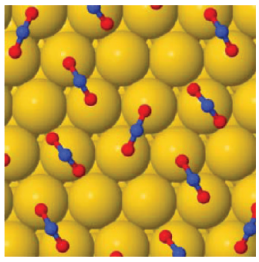

Figure 14. Model used for DFT calculations of the decorated ⟨2 1 −3⟩ boundaries in the STM image of Figure 9. The ($\sqrt{7} \times \sqrt{7}$)R19.1° unit mesh contains three NO_2 molecules, giving a coverage of 0.43 ML.

CONCLUSIONS

NO_2 adsorbs molecularly on Au{111} at 78 K, initially as small clusters at the elbows of the type-x reconstruction lines of the clean-surface herringbone reconstruction, and then as larger clusters on the fcc regions between the "pinched" elbows. With increasing exposure, islands of NO_2 grow on the fcc regions. These islands contain small domains of a well-ordered ($\sqrt{3} \times 2$)rect.-NO_2 structure with 0.25 ML local coverage. The islands grow and coalesce with increasing exposure, lifting the herringbone reconstruction and leading to the formation of strings of Au nanoclusters. By 0.25 ML overall coverage, the entire surface is covered with an NO_2 overlayer, predominantly composed of the ($\sqrt{3} \times 2$)rect. structure but with various point and line defects leading to a degree of disorder, as well as Au nanocluster strings. The disorder increases with further exposure beyond the 0.25 ML point, with the onset of multilayer formation estimated to occur above around 0.43 ML.

The NO_2 molecules occupy bridge sites, bonding to the surface through their O atoms in a chelated configuration. In the ($\sqrt{3} \times 2$)rect. phase at 0.25 ML, the molecules adopt the "rotated-molecule" arrangement indicated in Figure 6, with a binding energy of 0.821 eV, some 15% of which is accounted for by van der Waals interactions. The calculations indicate only marginal destabilization with increasing coverage up to 0.5 ML, which is consistent with the experimental observation of single-layer coverage up to 0.43 ML. Certain structural aspects of the line defects observed by STM, however, are not fully captured by the calculations, even at the highest level of DFT currently available.

ASSOCIATED CONTENT

Supporting Information

Schematic structural models for the boundaries in Figures 7 and 8; for the region of surface in Figure 9; and for a typical region of Figure 5. This material is available free of charge via the Internet at http://pubs.acs.org.

AUTHOR INFORMATION

Corresponding Author

*Tel.: +44 (0)1223 336503; fax: +44 (0)1223 336362; e-mail: smd37@cam.ac.uk.

Present Addresses

[†]Petrochemical Research Institute, Petrochina Company Limited, Chaoyang District, Beijing, People's Republic of China.

‡Smith School of Enterprise and the Environment, University of Oxford, Hayes House, 75 George Street, Oxford OX1 2BQ, United Kingdom.

Notes

The authors declare no competing financial interest.

■ ACKNOWLEDGMENTS

We acknowledge financial support from the Engineering and Physical Sciences Research Council, Toyota Motor Corporation (TZ), and the Swiss National Science Foundation (MS).

■ REFERENCES

(1) Zhang, T; Liu, Z.-P.; Driver, S. M.; Pratt, S. J.; Jenkins, S. J.; King, D. A. *Phys. Rev. Lett.* **2005**, *95*, 266102.
(2) Driver, S. M.; Zhang, T.; King, D. A. *Ang. Chem. Int. Ed* **2007**, *46*, 700.
(3) Haruta, M. *Catal. Today* **1997**, *36*, 153.
(4) Valden, M.; Lai, X.; Goodman, D. W. *Science* **1998**, *281*, 1647.
(5) Hashmi, A. S. K.; Hutchings, G. J. *Angew. Chem., Int. Ed.* **2006**, *45*, 7896.
(6) Clarke, S. J.; Segall, M. D.; Pickard, C. J.; Hasnip, P. J.; Probert, M. J.; Refson, K.; Payne, M. C. *Z. Kristallogr.* **2005**, *220*, 567.
(7) Hedgeland, H.; Lechner, B. A. J.; Tuddenham, F. E.; Jardine, A. P.; Allison, W.; Ellis, J.; Sacchi, M.; Jenkins, S. J.; Hinch, B. J. *Phys. Rev. Lett.* **2011**, *106*, 186101.
(8) Sacchi, M.; Jenkins, S. J.; Hedgeland, H.; Jardine, A. P.; Hinch, B. J. *J. Phys. Chem. C* **2011**, *115*, 16134.
(9) Inderwildi, O. R.; King, D. A.; Jenkins, S. J. *Phys. Chem. Chem. Phys.* **2009**, *11*, 11110.
(10) Sacchi, M.; Galbraith, M.; Jenkins, S. J. *Phys. Chem. Chem. Phys.* 2012, accepted.
(11) Perdew, J. P.; Wang, Y. *Phys. Rev. B* **1992**, *45*, 13244.
(12) Vanderbilt, D. *Phys. Rev. B* **1990**, *41*, 7892.
(13) Monkhorst, H. J.; Pack, J. D. *Phys. Rev. B* **1976**, *13*, 5188.
(14) Ortman, F.; Schmidt, W. G. *Phys. Rev. B* **2006**, *73*, 205101.
(15) Wang, J.; Koel, B. E. *J. Phys. Chem. A* **1998**, *102*, 8573.
(16) Bartram, M. E.; Koel, B. E. *Surf. Sci.* **1989**, *213*, 137.
(17) Sato, S.; Senga, T.; Kawasaki, M. *J. Phys. Chem. B* **1999**, *103*, 5063.
(18) Harten, U.; Lahee, A. M.; Toennies, J. P.; Wöll, Ch. *Phys. Rev. Lett.* **1985**, *54*, 2619.
(19) Wöll, Ch.; Chiang, S.; Wilson, R. J.; Lippel, P. H. *Phys. Rev. B* **1989**, *39*, 7988.
(20) Barth, J. V.; Brune, H.; Ertl, G.; Behm, R. J. *Phys. Rev. B* **1990**, *42*, 9307.
(21) Takeuchi, N.; Chan, C. T.; Ho, K. M. *Phys. Rev. B* **1991**, *43*, 13899.
(22) Narasimhan, S; Vanderbilt, D. *Phys. Rev. Lett.* **1992**, *69*, 1564.
(23) The bright lines in the STM images mark high points in the reconstructed surface layer, where Au atoms sit in bridge positions relative to the second layer, midway between regions of fcc and hcp stacking. Often misnamed "soliton walls", the lines are best thought of as a form of Shockley partial dislocation. Here we refer to them simply as "reconstruction lines". The distinction between "type-x" and "type-y" reconstruction lines, and how these relate to "pinched" and "bulged" elbows are discussed in ref 24.
(24) Chambliss, D. D.; Wilson, R. J.; Chiang, S. *Phys. Rev. Lett.* **1991**, *66*, 1721.
(25) Chambliss, D. D.; Wilson, R. J.; Chiang, S. *J. Vac. Sci. Technol. B* **1991**, *9*, 933.
(26) Voigtländer, B.; Meyer, G.; Amer, N. M. *Phys. Rev. B* **1991**, *44*, 10354.
(27) Stroscio, J. A.; Pierce, D. T.; Dragoset, R. A.; First, P. N. *J. Vac. Sci. Technol. A* **1992**, *10*, 1981.
(28) Woodruff, D. P.; Delchar, T. A. *Modern Techiques of Surface Science*, 2nd ed.; Cambridge University Press: Cambridge, 1994.
(29) Lu, X.; Xu, X.; Wang, N.; Zhang, Q. *J. Phys. Chem. A* **1999**, *103*, 10969.
(30) Doering, M.; Rust, H.-P.; Briner, B. G.; Bradshaw, A. M. *Surf. Sci.* **1998**, *410*, L736.
(31) Zhang, T.; King, D. A.; Driver, S. M. (to be published).